Deep Learning Based Cell Imaging with Electrical Impedance Tomography

Deep Learning Based Cell Imaging with Electrical Impedance Tomography

Zhou Chen, Yunjie Yang, Jiabin Jia
Agile Tomography Group, School of Engineering
The University of Edinburgh
Edinburgh, UK
y.yang@ed.ac.uk

Pierre Bagnaninchi
MRC Centre for Regenerative Medicine
The University of Edinburgh
Edinburgh, UK
Pierre.Bagnaninchi@ed.ac.uk

***Abstract*—Monitoring the 3-D cell culture process or drug responses non-destructively using Electrical Impedance Tomography (EIT) is an emerging topic in biomedical imaging. Significant efforts have been spent on developing EIT image reconstruction algorithms in order to achieve robust and high-quality cell imaging. The considerable computation time and imperfect image quality are the main issues of these conventional methods whereas the emergence of deep learning techniques point out a new direction due to its fast inferences on object detection, image segmentation and classification. In this paper, a novel deep learning architecture is proposed by adding a fully connected layer before a U-Net structure. This new architecture will first generate an initial guess of the conductivity distribution and then feed it to the following denoising model. A novel initialization strategy is also proposed to further help obtain this initial guess. The performance of the method is verified by simulation and experimental data. The results show that the proposed model outperforms the state-of-the-art EIT algorithms and can generalize well to reconstruct unseen cases consisting of human breast cancer cell pellet.**

***Index Terms*—cell imaging, deep learning, electrical impedance tomography, image reconstruction**

I. Introduction

IMAGING the process of 3-D cellular culture in a label-free, non-destructive way is increasingly attractive in the field of tissue engineering, especially for long-term biological behavior monitoring. Electrical Impedance Tomography (EIT) is a tomographic technique that images the cross-section distribution of conductivity within the Region of Interest (ROI) through measuring differential voltages at the boundary of the ROI which is covered by an electric field [1]. With its advantages of non-destructiveness, low-cost and radiation-free measurement, EIT in recent years has been particularly preferred and extensively exploited in cell culture imaging [2], breast cancer detection [3], rat brain imaging [4], etc.

Cell imaging with EIT has posed particular challenges in solving the EIT-image-reconstruction problem. The miniaturisation of the EIT sensor leads to much weaker measurement signals and the reconstruction method is required to be more robust to noise. In addition, the large amount of real-time data generated from the cell imaging processes requires computational cost-efficient methods. Although an increasing number of regularization-based image reconstruction algorithms have been proposed for normal-scale scenarios, e.g. Total Variation (TV) regularization [5], sparsity regularization [6] and pre-iterative Landweber [7]. These approaches are time-consuming and their noise resistance performance is not satisfactory in miniature EIT imaging, particularly cell imaging.

Data-driven or learning-based methods recently have been a new frontier for tomographic image reconstruction [8]. Though it usually takes a long time to train the model, incredibly fast inferences contribute to their growing popularity, which implies their potential in real-time imaging. Zheng et al. [9] proposed an auto-encoder structure for Electrical Capacitance Tomography (ECT) image reconstruction. Tan et al. [10] developed a LeNet-like network for Electrical Resistance Tomography (ERT). In these work, deep learning has demonstrated its superiority over conventional reconstruction methods as mentioned above. With respect to EIT, Hu et al. [11] introduced a Convolutional Neural Network (CNN) which blindly mapped specially rearranged measurement data to conductivity distribution. This method takes into account the geometrical structure inside measurement data from EIT sensors. However, to what extent this geometry information is learned by the network and thus benefits the solving of the inverse problem has not been investigated.

In this paper, a novel deep-learning based EIT image reconstruction algorithm is proposed particularly for cell imaging. The proposed method aims at forcing the network to make predictions step by step as a human does instead of a blind mapping. In this work, two steps are specified. As illustrated in Fig. 1, this network generates a plausible guess based on measured data at the first stage. After going through a denoising model, the image quality of the initial guess will be dramatically improved. Due to the limitation of dataset where the conductivity distribution only has two values, we consider to simplify the reconstruction task down to a two-class prediction problem: background and object.

Two main contributions of this work are summarised as follows:

1) A novel network architecture FC-UNet is proposed for EIT image reconstruction. A fully connected layer and a ReLU layer are added before a denoising network U-Net to generate the initial guess.

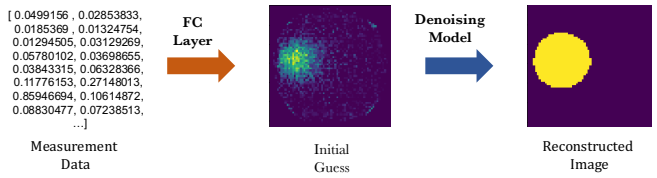

Fig. 1. The Processing Pipeline of FC-UNet.

2) Inspired by the concept of transfer learning, the first part of our network is initialized with a linear regression solution. This method is expected to reduce the training time and improve the performance of image reconstruction.

The FC-UNet model is verified using both simulation data and experimental data on MCF-7 human breast cancer cells to demonstrate its generalization ability.

II. Methodology

A. Electrical Impedance Tomography

The inverse problem of EIT is to compute the conductivity distribution based on induced voltage measurements. Usually the boundary voltage $\mathbf{V}$ is considered as a function of the conductivity distribution $\boldsymbol{\sigma}$ as

$$\mathbf{V} = F(\boldsymbol{\sigma}). \tag{1}$$

In practical, the linearized format of Eq. (1) is commonly adopted, which describes a small perturbation of conductivity distribution $\Delta\boldsymbol{\sigma}$ and the induced change of boundary voltage on electrode pairs $\Delta\mathbf{V}$. The linearized expression is given by

$$\Delta\mathbf{V} = \mathbf{J}\Delta\boldsymbol{\sigma} + \mathbf{e} \tag{2}$$

where $\mathbf{J}$ donates the Jacobian matrix (also known as the sensitivity matrix), and $\mathbf{e}$ is the measurement error or additional noise.

Typically the noise term $\mathbf{e}$ in Eq. (2) is neglected so that the inverse problem can be simplified to solve an approximated linear relationship [12]. In this work, the nonlinear relationship between $\Delta\mathbf{V}$ and $\Delta\boldsymbol{\sigma}$ is learned.

B. Network Architecture

As shown in Fig. 2, the architecture of our FC-UNet is designed having two sections: guessing and denoising. Inspired by Eq. (2), the initial guess about the conductivity distribution can be provided by some matrix multiplication. Since matrix multiplication is always implemented by introducing a fully connected layer in principle, we firstly have a fully connected layer followed by a ReLU layer.

In order to learn the denoising part, a UNet-like architecture is employed afterwards which was first proposed especially for biomedical image segmentation [13]. The main idea of U-Net is to map an image to a vector and then reconstruct it back to an image. The contraction on the left hand side applies two 3×3 convolutional layers with a 2×2 max pooling in each step whereas the layer at the bottom employs 2×2 upsample layer after convolutions. During expansion on the right hand side, the corresponding feature maps from the contraction part are reused to reduce distortion of images. They are appended directly after the upsample layer. After the two-convolution operation for the last step, a 1×1 convolutional layer and a sigmoid layer are used for classification.

Each pixel is eventually classified into either background or object. As only two classes are predicted, our loss function is defined using the concept of binary-cross-entropy.

C. Evaluation Metrics

In order to quantitatively evaluate the image reconstruction algorithms, relative image error (RIE) and correlation coefficient (CC) are selected as evaluation metrics, which are defined by

$$RIE = \frac{||\Delta\hat{\boldsymbol{\sigma}} - \Delta\boldsymbol{\sigma}||}{||\Delta\boldsymbol{\sigma}||} \tag{3}$$

$$CC = \frac{\sum_{i=1}^{N}(\Delta\hat{\sigma}_i - \overline{\Delta\hat{\boldsymbol{\sigma}}})(\Delta\sigma_i - \overline{\Delta\boldsymbol{\sigma}})}{\sqrt{\sum_{i=1}^{N}(\Delta\hat{\sigma}_i - \overline{\Delta\hat{\boldsymbol{\sigma}}})^2 \sum_{i=1}^{N}(\Delta\sigma_i - \overline{\Delta\boldsymbol{\sigma}})^2}} \tag{4}$$

where $\Delta\boldsymbol{\sigma}$ is the ground truth; $\Delta\hat{\boldsymbol{\sigma}}$ represents the predicted conductivity distribution; $\Delta\hat{\sigma}_i$ is the ith element of $\Delta\hat{\boldsymbol{\sigma}}$; $\Delta\sigma_i$ is the ith element of $\Delta\boldsymbol{\sigma}$; $\overline{\Delta\hat{\boldsymbol{\sigma}}}$ denotes the mean of $\Delta\hat{\boldsymbol{\sigma}}$, and $\overline{\Delta\boldsymbol{\sigma}}$ is the mean of $\Delta\boldsymbol{\sigma}$; N is the total number of pixels.

RIE and CC calculate the relative error and similarity between the true value and prediction, respectively.

III. Experimental Setup

A. Dataset

Dataset in this work are collected from [11], where 15,514 samples are used for training, 3,000 samples are used for validation and another 10,997 samples are used for testing. In training and validation data, samples contain 1, 2 and 4 round objects with random locations and radius within the sensing region. Testing data consist 1,2,3 and 4 round objects to verify the generalization ability of our algorithm.

In addition, noisy measurement data are appended to both training and validation data, which can enhance the robustness of our model when unavoidable noise or error is encountered. Signal-to-Noise Ratio (SNR) of 50dB is added to 5,000 samples from the training data and also 1,000 samples from the validation data. SNR of 40dB is added to another 5,000 and 1,000 samples from training and validation data respectively. Table I summarizes the details of each dataset.

B. Optimizer

Our model uses Adam [14] for optimization. The initial learning rate is 0.0001, which decays with a factor of 0.1. The model is trained with a batch size of 25. Experiments are implemented based on NVIDIA P5000 GPUs.

TABLE I
Number Of Samples In Each Dataset

Dataset	*Training*	*Validation*	*Testing*
Number of Objects	1,2,4	1,2,4	1,2,3,4
Number of Samples	25,514	5,000	10,997

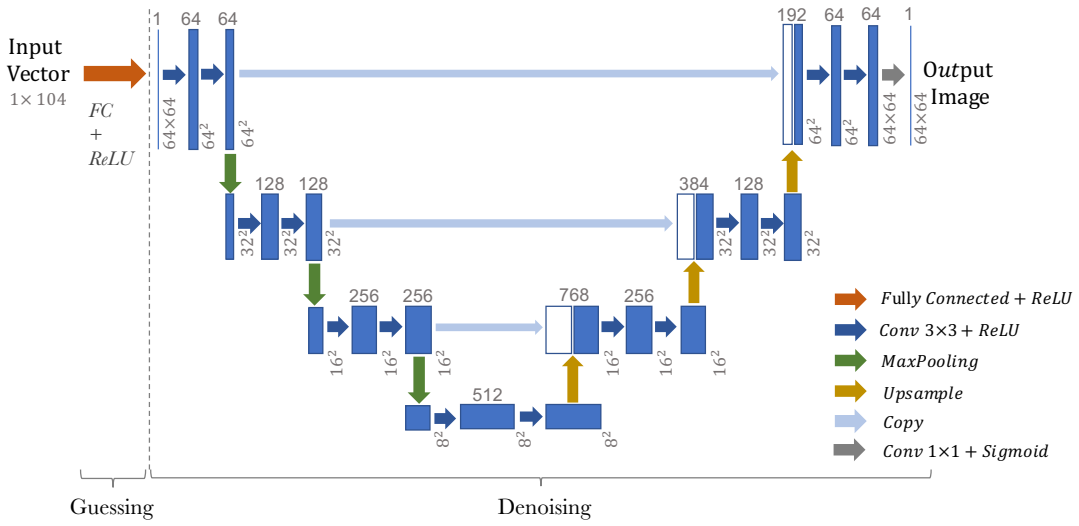

Fig. 2. The architecture of FC-UNet

C. Weight Initialization

What transfer learning does is to take a pre-trained model of one task as a starting point for another task. The more similar the two tasks, the better performance the new task will achieve compared to the model without transfer learning [15]. Consequently, we propose to initialize weights for the fully connected layer with the least-squares solution (LS) of the linear function $\Delta \mathbf{V} = \mathbf{J}\Delta\boldsymbol{\sigma}$ using training data, instead of random weights. In our work, this solution is given by a Numpy linear algebra function named 'numpy.linalg.lstsq'. During training, these weights keep being updated rather than frozen. The rest is initialized with random weights as usual.

We expect the rough solution from the above operation could provide a better starting point and easily lead to a global minimum rather than a local minimum.

For the baseline model whose structure is the same as that of FC-UNet, all weights are initialized randomly.

D. Early Stopping

The simplest way to determine the convergence of training is to set a threshold. Some researchers may choose a maximum training epoch. Our work takes advantage of early stopping, which stops the training process before the validation loss increases. Specifically, our model waits for 5 epochs after the latest minimum validation loss. Namely, if the performance on validation data keeps getting worse for certain epochs, the one with lowest validation loss is selected as the best model. The maximum number of epochs is set to be 50.

IV. Results and Discussions

A. Learning Curves

Learning curves shown in Fig. 3 compare different weight initialization methods as discussed in Section III-C. The training line in blue with LS solution as initialization has lower starting point and lower asymptote at the end compared to the training line in green with traditional random initialization. This implies that initialization based on LS results provides a preferable starting point for training, which helps the model learn much faster and also improves the performance.

The early stopping mechanism is also presented in Fig. 3. The orange and red lines stands for the validation curves for initialization with LS solution and random weights respectively. In early stages, the validation loss in each case is smaller than the training loss. This means more training is required since the model underfits the training data. After 4 epochs, the training loss starts exceeding the validation loss. The dashed line in grey and the one in yellow indicate that our method stops the training process at the 11th epoch whereas the baseline method stops at the 16th epoch. Obviously, the LS initialization method reduces significantly the training time and demonstrates much better validation performance, when compared to the random initialization strategy.

B. Image Reconstruction with Simulation Data

The FC-UNet model is compared with three state-of-the-art EIT image reconstruction algorithms, i.e. the regularization algorithm L1 [16], sparse Bayesian learning (SBL) [17] and adaptive group sparsity (AGS) [1]. To ease comparisons, estimated conductivity distributions based on L1, SBL and AGS are all normalized.

Row (b) in Fig. 4 qualitatively validates the effectiveness of the proposed initialization method which is highlighted in Section III-C, predicting an unseen 3-circle case from testing data. This method follows a human approach to reasoning in that we humans tend to start with an initial guess given a problem and then improve our guess with more specific knowledge in certain field. Even if the baseline model eventually achieves a similar result to the ground truth, its hidden-layer feature after the fully connected layer or initial guess seems like a random noise thus is not explainable to us. One possible reason is that it falls into a local minimum when conducting this first guess.

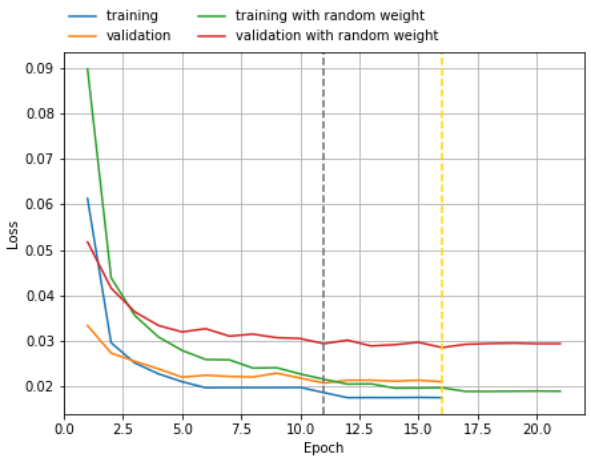

Fig. 3. The learning curves illustrate the difference between initialization with LS solution and random weights for the fully connected layer as well as the early stopping mechanism.

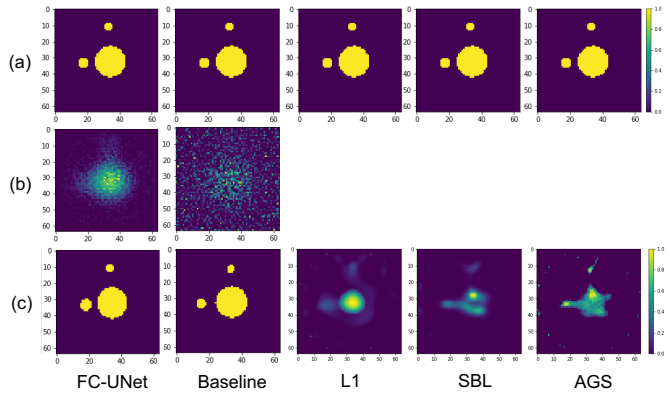

Fig. 4. Image reconstruction results of an unseen 3-circle case based on five algorithms. (a) Ground truth (same for each algorithm) (b) Corresponding initial guess for FC-UNet and the baseline model (c) Corresponding final results

In contrast, our FC-UNet is more reliable when we look into how it learns step by step. Consequently we believe FC-UNet is able to make plausible predictions on objects with more complicated shapes. Row (c) in Fig. 4 further demonstrates the superiority of deep learning based image reconstruction methods against other traditional methods. The surrounding electrodes are unexpectedly recognized by L1 and AGS.

Despite the above achievement, due to the limitation of dataset where only binary reconstructed images are provided, same conductivity level for each object is not suitable to distinguish in between objects.

Quantitatively, Table II and Table III compare the average RIE and CC of the testing data respectively when various noise levels are added to measurements. Among all, results of FC-UNet have the lowest RIE of 0.2597 without noise, 0.3619 with 50dB noise, 0.4913 with 40dB noise, and 0.7938 with 30dB noise. FC-UNet also achieves the highest CC in different cases, which is 0.9227, 0.8507, 0.7457 and 0.5193 with no noise, SNR of 50dB, 40dB and 30dB, respectively.

TABLE II
COMPARISON OF RIE AT VARIOUS NOISE LEVELS

Image Reconstruction Algorithm	SNR			
	Noise Free	*50dB*	*40dB*	*30dB*
L1 [16]	0.8114	0.8057	0.8054	0.8378
SBL [17]	0.8744	0.8754	0.8834	0.9340
AGS [1]	0.8598	0.8600	0.8620	0.8719
Baseline	0.3361	0.3899	0.5065	0.8055
FC-UNet	**0.2597**	**0.3619**	**0.4913**	**0.7938**

TABLE III
COMPARISON OF CC WITH VARIOUS NOISE LEVELS

Image Reconstruction Algorithm	SNR			
	Noise free	*50dB*	*40dB*	*30dB*
L1 [16]	0.6712	0.6669	0.6674	0.6591
SBL [17]	0.5626	0.5626	0.5590	0.5341
AGS [1]	0.5367	0.5368	0.5345	0.5273
Baseline	0.8794	0.8347	0.7358	0.3759
FC-UNet	**0.9227**	**0.8507**	**0.7457**	**0.5193**

TABLE IV
COMPARISON OF AVERAGE INFERENCE TIME

L1 [16]	***SBL*** [17]	***AGS*** [1]	***Baseline***	***FC-UNet***
7.22s	91.76s	9.89s	11.24ms	10.62ms

In terms of time assumption, FC-UNet achieves the fastest average inference time of 10.62ms as shown in Table IV.

C. Image Reconstruction with Experimental Data

The performance of FC-UNet presented in Section IV-B is further evaluated with experimental data, i.e. EIT measurements of MCF-7 human breast cancer cell line aggregates. A 16-electrode quasi-2D micro EIT sensor designed by the authors [18] is employed, which is able to incorporate impedance sensing with prevailing optical imaging modalities for cellular imaging. The schematic and manufactured miniature EIT sensor are presented in Fig. 5. The sensing chamber has a diameter of 14mm and a height of 1.6mm. MCF-7 human breast cancer cells aggregates with a diameter of approximately 2mm are the objects to be imaged.

Five different distribution phantoms are examined as shown in Fig. 6, where two cell aggregates are involved in each case. Compared to the ground truth in the first row, the initial guesses from the second row seem plausible as they offer a

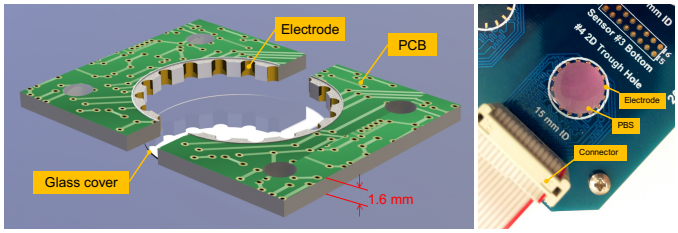

Fig. 5. The schematic and manufactured quasi-2D micro EIT sensor [18].

rough idea about the conductivity distribution in each case. The final image reconstruction results of phantom 1, 2 and 3 in the third row demonstrate strong denoising capability of FC-UNet. It is noted that when the two cell spheroids become closer in phantom 4 and 5, the FC-UNet still manages to separate them clearly even though the initial guesses have mistakenly made a single-object prediction. That is to say, multi-object detection in micro scale is promised and their locations are estimated stably while the FC-UNet was trained with simulated measurements under conventional EIT setup. Though a shortage is the imperfect size of the reconstructed cell spheroids, the proposed method is of great potential to facilitate robust and high-resolution cell imaging with micro EIT sensors.

V. Conclusions

In this paper, a novel deep learning approach based on FC-UNet is proposed for cell imaging with micro EIT sensors. The main contribution is to add a fully connected layer and a ReLU layer ahead of a denoising model that is similar to U-Net. This method paired with a special weight initialization strategy is proved to be feasible to provide an plausible initial guess according to both simulation and experimental validations. The image reconstruction results based on simulation data quantitatively shows the ascendancy of deep learning approaches. The performance on EIT measurements of MCF-7 human breast cancer cell line aggregates demonstrates the strong generalization ability of FC-UNet which manages to explicitly recognize multiple cells in an unseen micro scale.

References

[1] Yang Y, Jia J, “An image reconstruction algorithm for electrical impedance tomography using adaptive group sparsity constraint,” IEEE Transactions on Instrumentation and Measurement. 2017 May 23;66(9):2295-305.

[2] Yang Y, Jia J, Smith S, Jamil N, Gamal W, Bagnaninchi PO, “A miniature electrical impedance tomography sensor and 3-D image reconstruction for cell imaging,” IEEE Sensors Journal. 2016 Nov 21;17(2):514-23.

[3] Hong S, Lee K, Ha U, Kim H, Lee Y, Kim Y, Yoo HJ, “A 4.9 mΩ-sensitivity mobile electrical impedance tomography IC for early breast-cancer detection system,” IEEE Journal of Solid-State Circuits. 2014 Sep 29;50(1):245-57.

[4] Aristovich KY, Packham BC, Koo H, dos Santos GS, McEvoy A, Holder DS, “Imaging fast electrical activity in the brain with electrical impedance tomography,” NeuroImage. 2016 Jan 1;124:204-13.

[5] Wang H, Tang L, Cao Z, “An image reconstruction algorithm based on total variation with adaptive mesh refinement for ECT,” Flow Measurement and Instrumentation. 2007 Oct 1;18(5-6):262-7.

[6] Jin B, Khan T, Maass P, “A reconstruction algorithm for electrical impedance tomography based on sparsity regularization,” International Journal for Numerical Methods in Engineering. 2012 Jan 20;89(3):337-53.

[7] Wang H, Wang C, Yin W, “A pre-iteration method for the inverse problem in electrical impedance tomography,” IEEE Transactions on Instrumentation and Measurement. 2004 Jul 19;53(4):1093-6.

[8] Wang G, Ye JC, Mueller K, Fessler JA, “Image reconstruction is a new frontier of machine learning,” IEEE transactions on medical imaging. 2018 May 15;37(6):1289-96.

[9] Zheng J, Peng L, “An autoencoder-based image reconstruction for electrical capacitance tomography,” IEEE Sensors Journal. 2018 May 15;18(13):5464-74.

[10] Tan C, Lv S, Dong F, Takei M, “Image reconstruction based on convolutional neural network for electrical resistance tomography,” IEEE Sensors Journal. 2018 Oct 16;19(1):196-204.

[11] Hu D, Lu K, Yang Y, “Image reconstruction for electrical impedance tomography based on spatial invariant feature maps and convolutional neural network,” 2019. Paper presented at 2019 IEEE International Conference on Imaging Systems and Techniques , ABU DHABI, United Arab Emirates, in press.

[12] Lionheart WR, “EIT reconstruction algorithms: pitfalls, challenges and recent developments,” Physiological measurement. 2004 Feb 3;25(1):125.

[13] Ronneberger O, Fischer P, Brox T, “U-net: Convolutional networks for biomedical image segmentation,” In International Conference on Medical image computing and computer-assisted intervention 2015 Oct 5 (pp. 234-241). Springer, Cham.

[14] Kingma DP, Ba J, “Adam: A method for stochastic optimization,” In Proceedings of the International Conference on Learning Representations, 2015.

[15] Torrey L, Shavlik J, “Transfer learning,” InHandbook of research on machine learning applications and trends: algorithms, methods, and techniques 2010 (pp. 242-264). IGI Global.

[16] Jamil N, Yang Y, Tsiamis A, Jia J, Smith S, “Comparison of regularisation methods in image reconstruction for micro-bioimpedance tomography,” In2017 IEEE SENSORS (pp. 1-3). IEEE.

[17] Liu S, Jia J, Yang Y, “Image reconstruction algorithm for electrical impedance tomography based on block sparse Bayesian learning,” In 2017 IEEE International Conference on Imaging Systems and Techniques (IST) 2017 Oct 18 (pp. 1-5). IEEE.

[18] Yang Y, Wu H, Jia J, “Quasi-2D EIT-optical Dual Modality Sensor for Cellular Imaging,” ELECTRICAL IMPEDANCE TOMOGRAPHY. 2018 Jun.

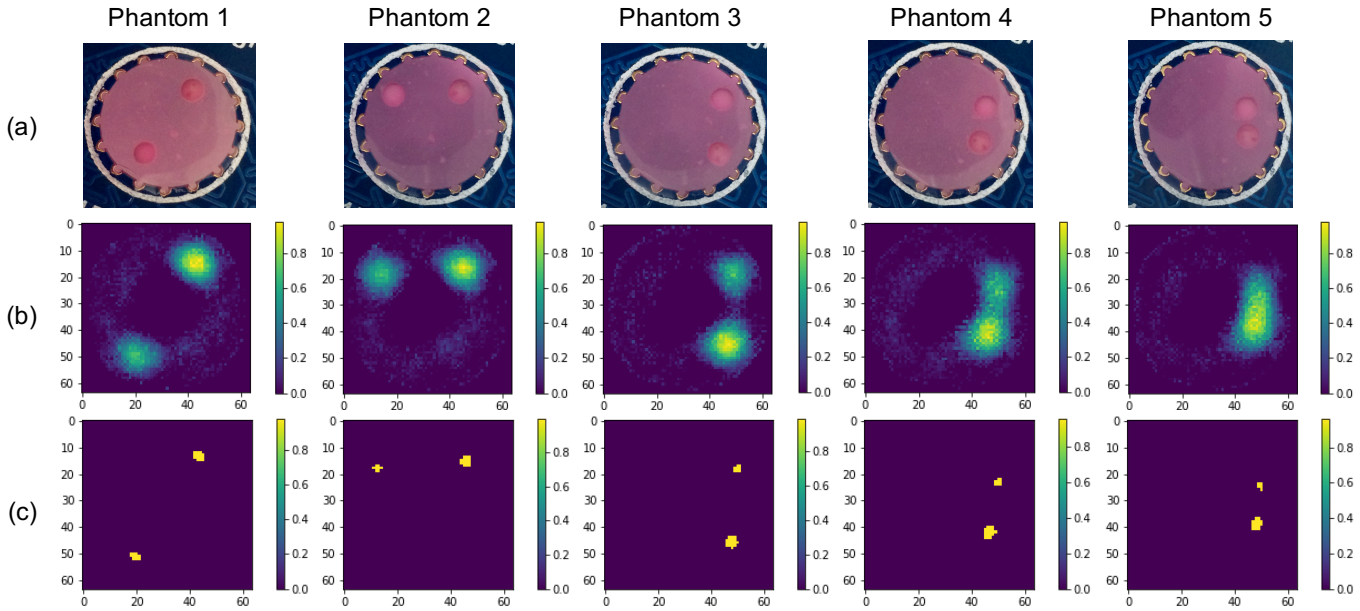

Fig. 6. Image reconstruction results of MCF-7 cell aggregates. (a) Five phantoms in micro scale showing the ground truth in each case. (b) Corresponding initial guess after the fully connected layer. (c) Corresponding results based on the full FC-UNet.